INL/RPT-22-70619
Rev. 0

Summary Report of INL Sensors and Instrumentation Activities in SPHERE and MAGNET

Changing the World's Energy Future

Idaho National Laboratory

INL/RPT-22-70619

Summary report of INL sensors and instrumentation activities in SPHERE and MAGNET

Troy Unruh
Joshua Daw
Kelly McCary

December 2022

Idaho National Laboratory
Idaho Falls, Idaho 83415

http://www.inl.gov

Prepared for the
U.S. Department of Energy
Office of NE
Under DOE Idaho Operations Office
Contract DE-AC07-05ID14517

Page intentionally left blank

ABSTRACT

This document provides a summary of Idaho National Laboratory sensor and instrumentation activities currently performed under the Department of Energy's (DOE's) Microreactor Program. These sensor and instrumentation capabilities, along with other laboratory capabilities, are available to support developer and other stakeholder needs. Specific experimental capabilities described in this document includes sensors and instrumentation for the single primary heat extraction and removal emulator (SPHERE) and the microreactor agile non-nuclear experimental test bed (MAGNET).

Page intentionally left blank

CONTENTS

1. INTRODUCTION 1
2. THERMAL AND HEAT TRANSFER TESTBEDS 1
2.1 INL Sensors and Instrumentation for the Single Primary Heat Extraction and Removal Emulator (SPHERE) Gap Conductance Test 1
2.1.1 Temperature Sensors used in SPHERE 4
2.1.2 Ultrasonic Thermometer (UT) Performance 5
2.1.3 Fiber Optic Sensor Performance 8
2.2 INL Sensor and Instrumentation for the Microreactor Agile Non-Nuclear Experimental Test Bed (MAGNET) 14
2.2.1 Sensor and Instrumentation for eBlock37 Heat Pipe Test Article 14
3. CONCLUSIONS 16
4. REFERENCES 16

FIGURES

Figure 1. Gap conductance test at the SPHERE test bed 2
Figure 2. Heat Pipe centerline thermocouple measurement points 2
Figure 3. Thermowell in sodium filled heat pipe 2
Figure 4. Drawing of hex block with notches 3
Figure 5. Hex block slot locations 3
Figure 6. Ultrasonic thermometer schematic. 4
Figure 7. UT temperature profiles for four atmospheres. 5
Figure 8. Comparison of temperatures measured by UT and TCs in Vacuum. 6
Figure 9. Comparison of temperatures measured by UT and TCs in Argon. 7
Figure 10. Comparison of temperatures measured by UT and TCs in Nitrogen. 7
Figure 11. Comparison of temperatures measured by UT and TCs in Helium. 8
Figure 12: Response of DTS fiber and thermocouples at various location along the hex block. 9
Figure 13: DTS fiber and thermocouple response at steady state with a helium gas fill. 9
Figure 14: Full profile of the hex block over the duration of the helium fill test. 10
Figure 15: DTS fiber profile of the hex block at each of the three steady state holds for the helium gas fill. 11
Figure 16: Initial steady state hold with argon fill gas. 12
Figure 17: Temperature spike for argon fill gas heat-up. 12
Figure 18: Full profile of the hex block until sensor failure of the argon fill test. 13

Figure 19: DTS fiber profile of the hex block at various times for the argon gas fill. 14
Figure 20 Cross section of the eBlock37 core37 block 15
Figure 21. Possible locations for use of ultrasonic thermometer. 15
Figure 22: Possible locations for use of DTS or FBG fibers. 16

TABLES

Table 1. Tabulated temperatures from UT. 6

Page intentionally left blank

Summary report of INL sensors and instrumentation activities in SPHERE and MAGNET

1. INTRODUCTION

This document provides a summary of Idaho National Laboratory sensor and instrumentation activities currently performed under the Department of Energy's (DOE's) Microreactor Program to provide information on the work being done by the program that is of interest for microreactor research and development. These sensor and instrumentation capabilities, along with other laboratory capabilities, are available to support developer and other stakeholder needs (Sabharwall 2021).

2. THERMAL AND HEAT TRANSFER TESTBEDS

The primary experimental hardware capabilities for sensor and instrumentation demonstration and deployment are focused on non-nuclear thermal testing using various test articles to perform experiments. Specifically, this includes the single primary heat extraction and removal emulator (SPHERE) (Sabharwall 2020)and the microreactor agile non-nuclear experimental test bed (MAGNET) (Morton 2020).

The sensor and instrumentation capabilities described in this report can be made available to researchers and developers for a range of testing purposes. Those needing access to them or requiring other experimental capabilities and data are encouraged to reach out to the Microreactor Program National Technical Director. Full contact information is available on the program website: https://gain.inl.gov/SitePages/MicroreactorProgram.aspx

2.1 INL Sensors and Instrumentation for the Single Primary Heat Extraction and Removal Emulator (SPHERE) Gap Conductance Test

The objective of the SPHERE gap conductance test was to obtain data on the heat losses through the annular gap (0.025-inches radially) formed by the outer wall of the heat pipe and the inner diameter of a stainless-steel core block through radiative and conductive heat transfer with varying gas compositions. This experiment further demonstrates the heat transfer within a simulated microreactor environment to gain addition understanding of larger microreactor system under different gas compositions.

The SPHERE facility consists of multiple 12-inch diameter stainless steel sanitary tubes to allow for coupling with a wide variety of experiments. For the gap conductance test, inside the tubing was a core block wrapped with insulation and a layer of heat trace. Cartridge heaters were used to heat the core block and test article. In this case, the test article was a sodium filled heat pipe. The heat pipe ran the entire length of the sanitary tube setup. The heat pipe was also wrapped insulation and heat trace. The end of the heat pipe was coupled with a gas gap calorimeter for heat removal. A drawing of the gap conductance test is shown in Figure 1 below.

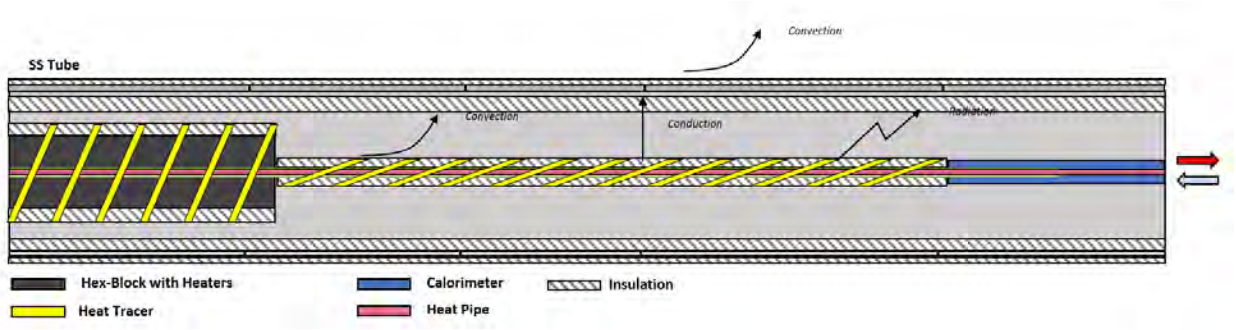

Figure 1. Gap conductance test at the SPHERE test bed

The test article is a sodium filled heat pipe supplied by Advanced Cooling Technologies (ACT) that was rated to an upper power limit of 1kW. The heat pipe has an outer diameter of 0.625-inch and wall thickness of 0.028-inch. The center of the heat pipe consists of an annular wick structure and a center region for the vapor to flow. The heat pipe has a centerline thermowell for the vapor region as shown in Figure 3. The thermowell outer diameter was 0.165-inch and the inner diameter was 0.135-inch. A multi-point thermocouple soured from Idaho Laboratory Corporation was inserted into the thermowell. The distances to the measurement points of the thermocouple are shown in Figure 2.

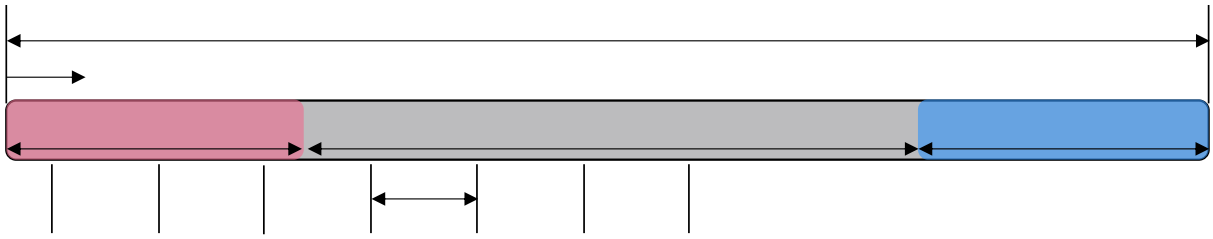

Figure 2. Heat Pipe centerline thermocouple measurement points

Figure 3. Thermowell in sodium filled heat pipe

The core block for this experiment was a 19.5-inch-long hex block made from 316-stainless steel as shown in Figure 4. The heat pipe was inserted into the hex block that was designed to simulate a subsection of common microreactor designs. To facilitate the installation of sensors and instrumentation, the hex block was machined using wire EDM (electrical discharge machining) to notch out sections of the heater holes as well as the center hole. The slots were filled with multipoint, type K thermocouples, fiberoptic temperature sensors, and an ultrasonic temperature sensor. The locations of the sensors are shown in Figure 5. Slots A, B, C, D, and E were used for the multipoint thermocouples. The remaining three slots were used for the two fiberoptic sensors and an ultrasonic sensor, respectively.

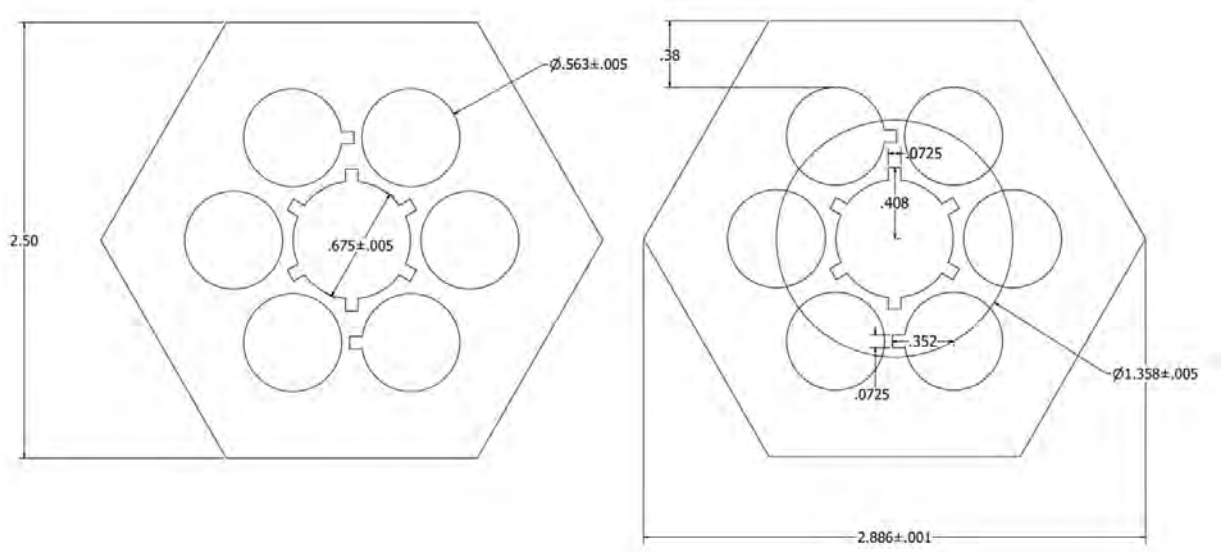

Figure 4. Drawing of hex block with notches

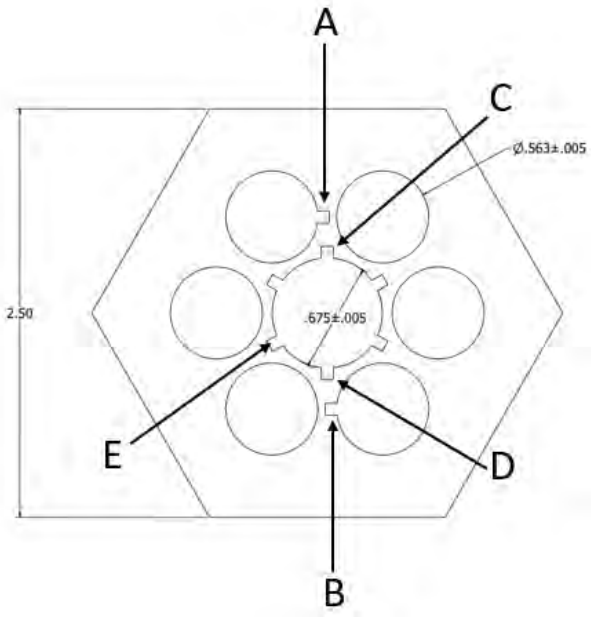

Figure 5. Hex block slot locations

2.1.1 Temperature Sensors used in SPHERE

The multipoint type K thermocouples were procured from Idaho Laboratory Corporation with 5 measurement points. The first point was located at the front end of the core block towards the adiabatic region of the heat pipe. The other points were located 3-inches after the first point. Standard calibration curves for type K thermocouples were applied.

The fiberoptic sensors ran down the axial length of the heat pipe which is in the center hole of the hex block. The sensors were able to record data down the entire length of the hex block for a total measured length of 19.5-inches. There were two types of fiberoptic sensors used for this experiment. The first was a fiber Bragg grating (FBG) sensor with 9 FBGs distributed equally throughout the fiber and the other was an optical frequency domain reflectometry (ODFR) distributed temperature sensor (DTS) with a spatial resolution of a data point every 0.65 mm (0.0256-inch). Both types of optical-fiber-based sensors chosen for deployment in the SPHERE facility have been previously demonstrated in-pile in the Transient Reactor Test Facility reactor (McCary 2017). The FBG sensor allows for measurements up to 1 kHz with a lower spatial resolution, only measuring at the locations of the FBGs but providing a more stable measurement at higher temperatures, above 700°C (Grobnic, 2006). The DTS fiber will fail above 700°C without the use of an adaptive reference technique to account for increased oxygen mobility at higher temperatures (Sweeney, 2020). The data acquisition system for the DTS fiber was the Luna Innovations ODiSI, this system allows for the high spatial resolution measurements as well as faster acquisition rate at the expense of using an adaptive measurement reference technique. The DTS fiber is an unaltered germanium doped silica fiber with a gold metal coating the manufacturer specified temperature limit for the coating is 600°C Both fibers have been installed in 0.063 in.-OD × 0.010in. wall stainless steel tubes to aid in installation and removal.

The ultrasonic thermometer (UT) is a temperature measurement sensor capable of measuring the temperature profile along the length of the sensor (Daw 2018). The UT was designed with five measurement zones and a total sensor length of fifteen inches (three inches per segment). The UT utilizes a magnetostrictive alloy to generate and sense ultrasonic waves in a waveguide, which is used as the sensor (Figure 6). Two UTs were built for the experiment, one using molybdenum waveguides and one with stainless steel waveguides. Each UT used two waveguides, each segmented with three laser welded bumps along the length of the UT. As there ended up being room for only one UT, the one with stainless steel waveguides was chosen, as stainless steel has a higher temperature sensitivity than molybdenum. The temperature is correlated to changes in the speed of sound in the waveguide material and can be measured using acoustic time domain reflectometry. The UT was intended to measure temperature along the entire length of the hex block coaxial to the heat pipe but due to a late experimental design change, only three of five segments were fully inserted into the block. The UT was able to record a sweep of data at 10Hz, one hundred times for each steady state condition that was reached during the experiment. This allowed for the data that was collected with the UTto be concise as the steady state data was the only area of interest for this experiment.

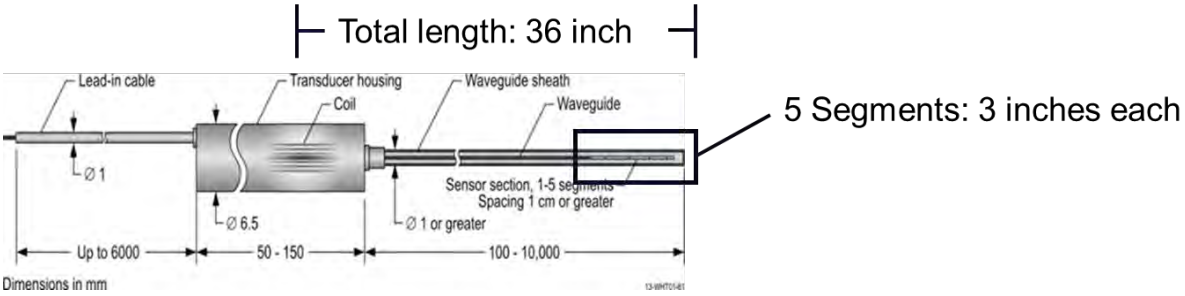

Figure 6. Ultrasonic thermometer schematic.

A LabVIEW virtual instrument was used for all data acquisition and instrument control. The system was equipped with a roughing pump to accomplish gas purging as needed and to allow the system to obtain a rough vacuum of approximately 25torr.

2.1.2 Ultrasonic Thermometer (UT) Performance

There were two issues with the data collected with the UT. First was the presence of an environmental RF noise which interfered with and partially obscured the recorded signal. At power levels of 500 W and below this had a minor effect, but at higher power levels the noise made the recorded signal unusable. The second issue was a problem with the initial calibration of the UT. As the UT measures an average temperature of each segment, it is critical for the UT segments to be isothermal during calibration. The furnace used for this calibration was too short to calibrate the full length of the UT. As a result, the initial processed temperatures were lower than expected. To correct this, the data was reprocessed using older calibration data from the same material stock that the waveguides were made from. Temperature profiles are shown in Figure 7. Segments 1 and 2 were not inserted into the block, segment 5 is the segment inserted the furthest. The recorded temperatures are shown in Table 1.

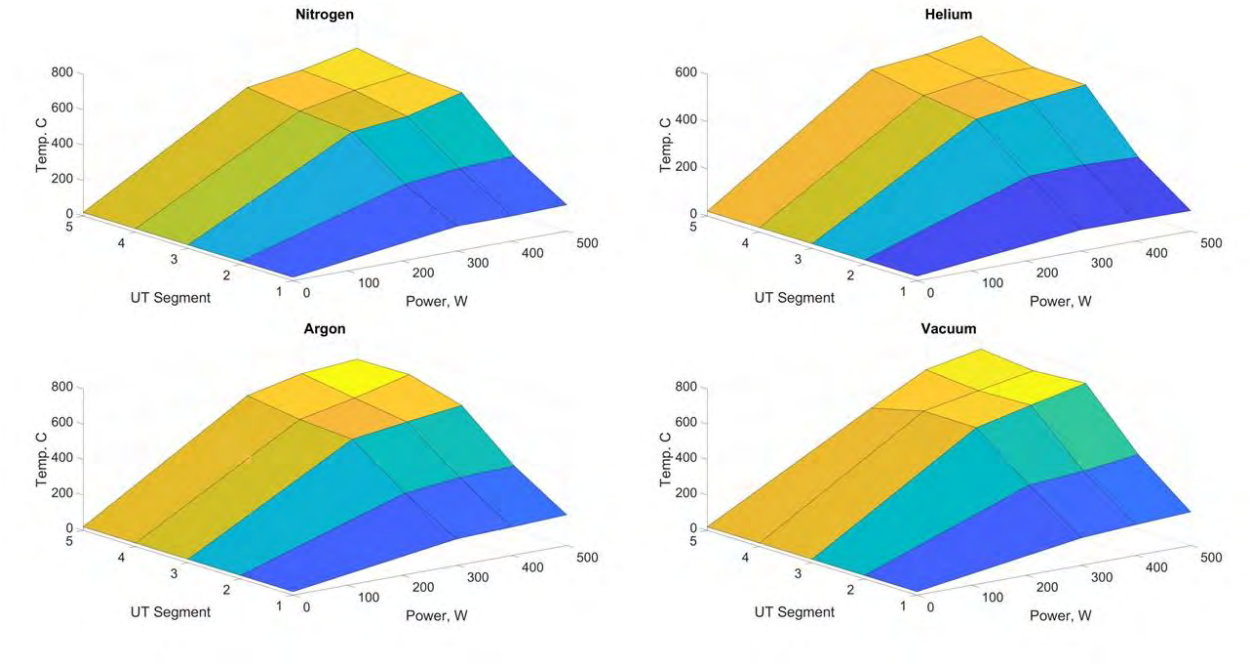

Figure 7. UT temperature profiles for four atmospheres.

Table 1. Tabulated temperatures from UT.

Argon	Power	Segment 1, ℃	Segment 2, ℃	Segment 3, ℃	Segment 4, ℃	Segment 5, ℃
	500 W	173.36	357.74	607.95	690.92	685.40
	400 W	160.19	348.28	570.94	614.14	660.48
	300 W	150.13	315.42	529.31	548.69	592.07
	0 W	19.81	19.80	19.80	19.80	19.80
Nitrogen	Power	Segment 1, ℃	Segment 2, ℃	Segment 3, ℃	Segment 4, ℃	Segment 5, ℃
	500 W	148.34	331.90	599.02	618.73	667.25
	400 W	141.10	319.65	520.73	576.72	599.10
	300 W	140.06	285.25	489.35	515.75	556.92
	0 W	19.81	19.80	19.80	19.80	19.80
Helium	Power	Segment 1, ℃	Segment 2, ℃	Segment 3, ℃	Segment 4, ℃	Segment 5, ℃
	800 W	No Data	No Data	No Data	No Data	No Data
	700 W	No Data	No Data	No Data	No Data	No Data
	600 W	No Data	No Data	No Data	No Data	No Data
	500 W	86.48	244.44	482.07	486.87	551.90
	400 W	89.22	253.92	456.77	485.04	516.03
	300 W	89.89	247.61	420.69	452.94	493.25
	0 W	19.81	19.80	19.80	19.80	19.80
Vacuum	Power	Segment 1, ℃	Segment 2, ℃	Segment 3, ℃	Segment 4, ℃	Segment 5, ℃
	500 W	189.42	422.23	733.01	712.26	742.94
	400 W	173.80	384.43	665.63	655.61	682.39
	300 W	154.98	360.76	594.20	596.53	522.10
	0 W	19.81	19.80	19.80	19.80	19.80

Figure 8 through Figure 11 show a comparison of the measured UT temperatures compared to the two nearest multipoint TCs (C and E). As the UT was not fully installed into the evaporator, the position relative to the TCs was estimated. Also, unlike the TCs, the UT does not truly measure temperature at a point. Rather, the average temperature between points is what is measured.

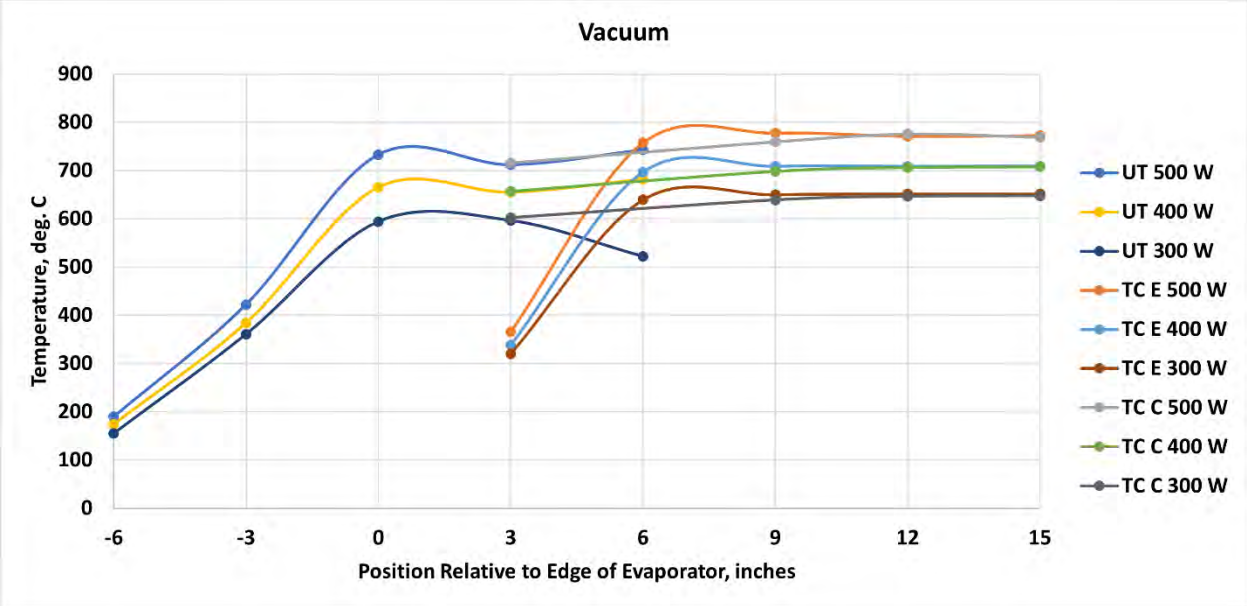

Figure 8. Comparison of temperatures measured by UT and TCs in Vacuum.

Figure 9. Comparison of temperatures measured by UT and TCs in Argon.

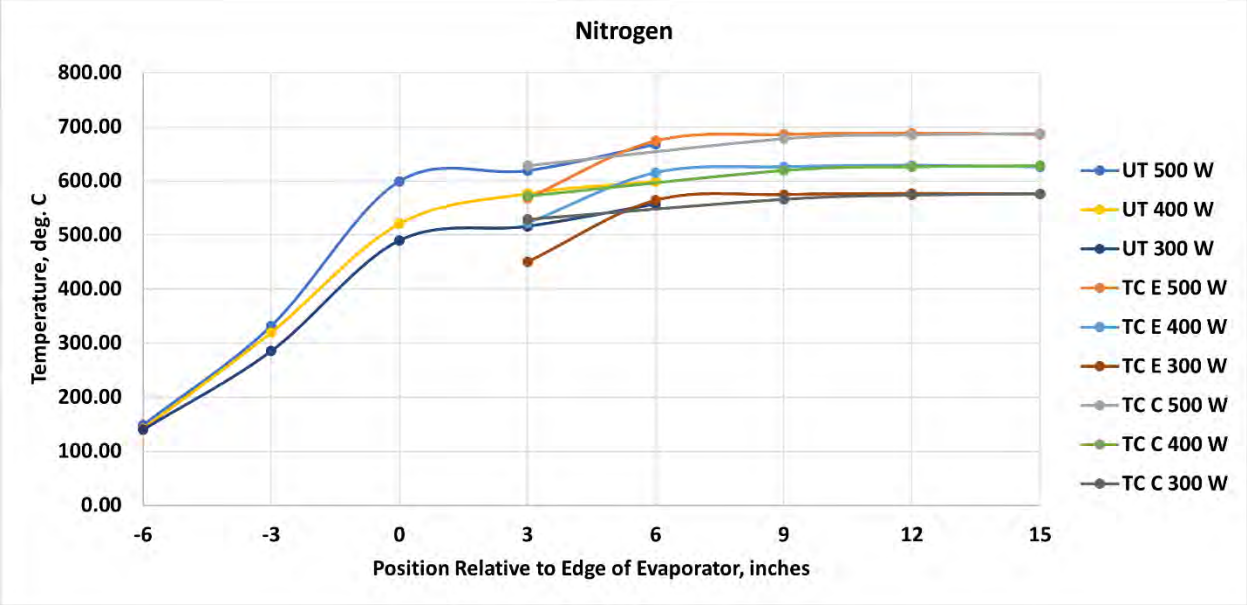

Figure 10. Comparison of temperatures measured by UT and TCs in Nitrogen.

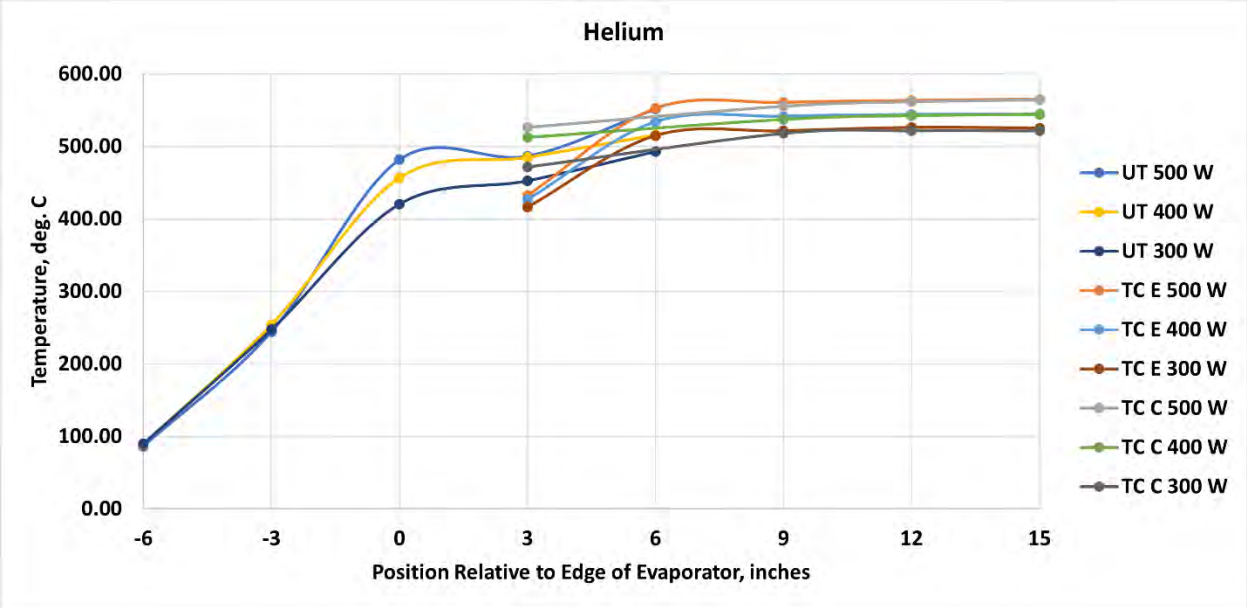

Figure 11. Comparison of temperatures measured by UT and TCs in Helium.

Despite ambiguity of the relative position of sensing locations and some anomalous behavior at the edge of the heating block, there is good agreement between UT and TC measurements within the block. If the UT is used in future testing or application, more care must be given to the calibration of the UT and to shielding the magnetostrictive transducer from external RF noise sources. If the RF noise can be isolated or removed, the UT would be ideal for use in temperatures exceeding those at which the multipoint TCs may be used (i.e., in excess of 1000 ℃).

2.1.3 Fiber Optic Sensor Performance

There were several challenges related to the fiber optic sensor data. First, the two sensors used two different acquisition systems, one of the systems had a failure that resulted in the loss of data for the FBG sensor. The next challenge was in the temperature and the length of time that the sensor was at temperature. The DTS fiber is based on a referencing scheme to the baseline measurement, this makes the measurement sensitive to defect migration, annealing, and density changes that occur within the fiber. This makes the pre-deployment thermal anneal of the significant to the performance of the sensor. The DTS fiber was annealed at 700°C for several hours to anneal out any low energy defects prior to taking the reference measurement. The gold coated fiber has a manufacturer specified limit of 600°C, however initial testing of the sensor in lab showed that the fiber would perform up to 700°C for 6-8 hours. Defect migration can still be an issued at long times held at high temperatures, if this is the mechanism of failure this can be overcome by re-referencing the fiber (at a known temperature), such as letting the entire system cool down to room temperature then refencing the fiber before re-heating, or by using an iterative referencing scheme. The current data acquisition system does not allow for the adaptive referencing scheme and the test operators did not want to cool completely to room temperature for the duration of the test to avoid unnecessary stress on the heaters in the system.

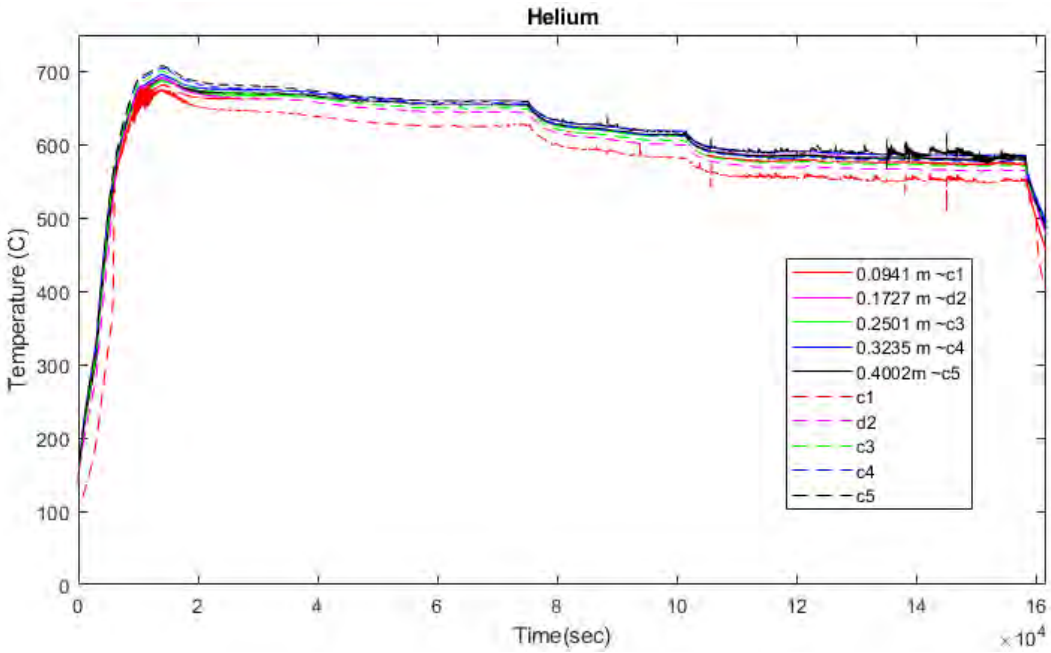

Figure 12: Response of DTS fiber and thermocouples at various location along the hex block.

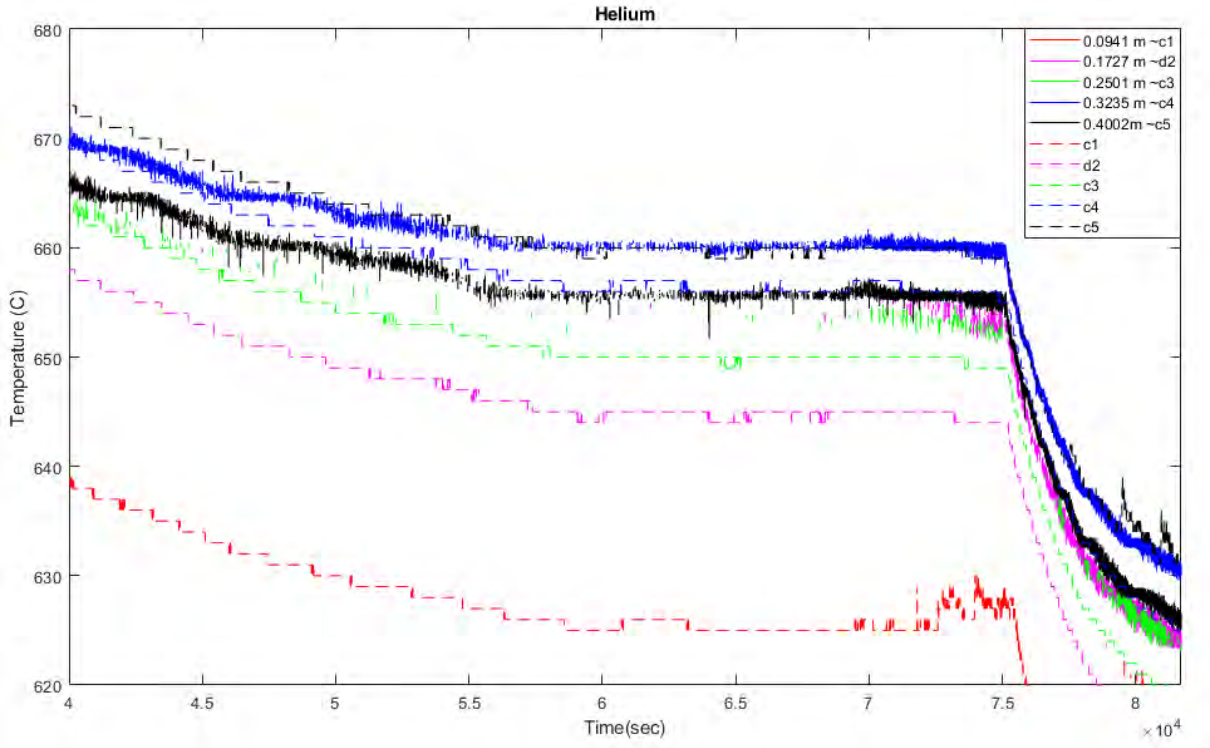

Figure 13: DTS fiber and thermocouple response at steady state with a helium gas fill.

The first fill gas tested was helium, Figure 12 shows the response of the DTS fiber at the approximate locations of the thermocouples over the duration of the helium fill test. Figure 13 is zoomed in on the first steady state hold with the helium fill gas. The dotted lines are thermocouples at various location along the hex block. the fiber traces at estimated to be at approximately the same locations as the thermocouples. The locations close to the edge of the block have the biggest temperature difference, this could be due to the

ambiguity in the locations. The measurements towards the center of the hex block better match the thermocouples, the location dependence of the sensors is less significant towards the center of the hex block. The measurements towards the center of the block are within 5°C of each other. The first steady state hold of the helium was already approximately 16 hours into the test at high temperatures.

In Figure 12 and Figure 13 the signal for the fiber is dropping in and out, this is likely due to an inability to reference the active scan back to the baseline scan. Figure 14 shows a surface plot of the for the helium fill test. This shows the dropouts of the fiber measurement and some of the recoveries. The referencing issue maybe caused by defect migration or by stresses on the fiber with relation to the coating on the fiber. There is some recovery of the measurements at lower temperatures, this may be due to the stresses relaxing at the lower temperatures. The profile of the hex block at each of the steady state holds for the helium gas fill can be seen in Figure 15. The hex block on the evaporator side starts at length 0 and ends at 0.495 meter (19.5 inches), the DTS fiber extends a small distance past the hex block. The profile measurement shows a flat temperature profile, which is expected, and a small drop in temperature past the hex block on top just the heat pipe. If there were a significant hot spot the distributed sensor would show that where a multipoint thermocouple may not be located.

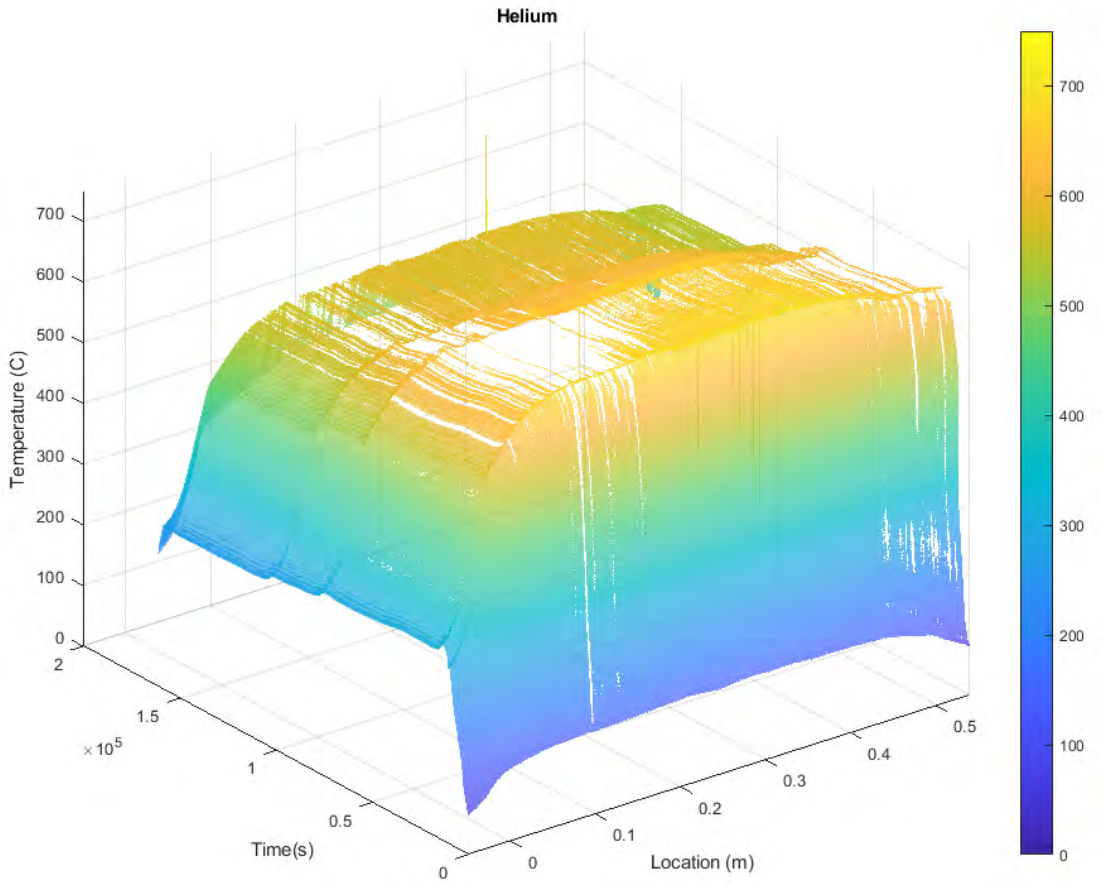

Figure 14: Full profile of the hex block over the duration of the helium fill test.

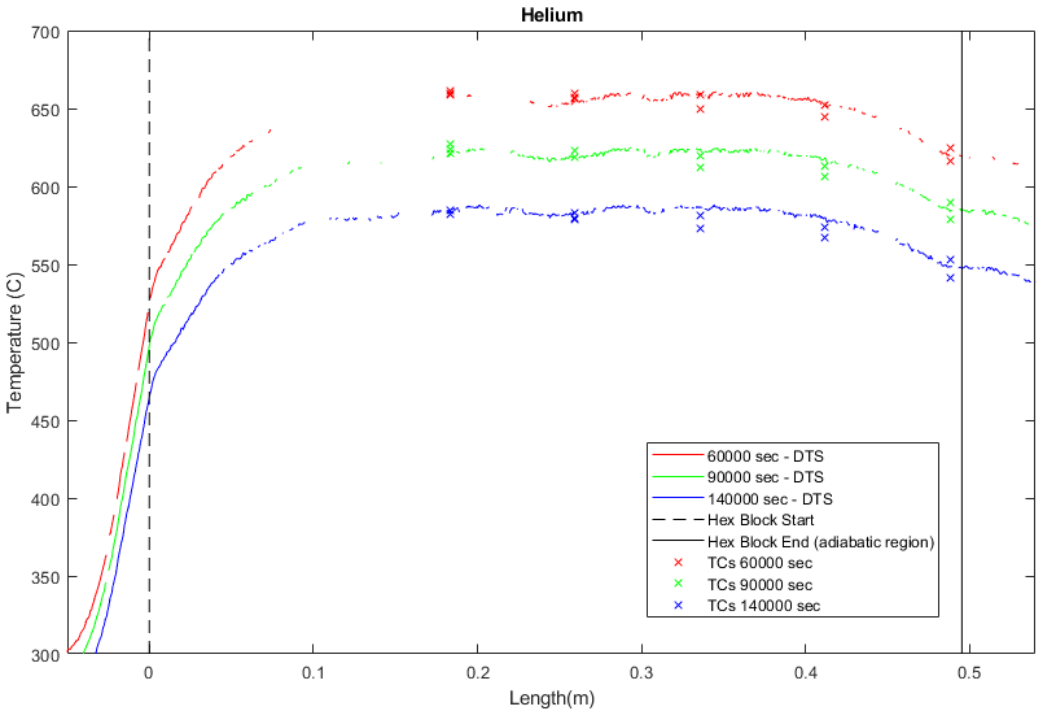

Figure 15: DTS fiber profile of the hex block at each of the three steady state holds for the helium gas fill.

The initial heat up for the argon gas fill heated to above 750°C, this temperature spike caused a failure in the sensor. Figure 16 show the temperature spike and the first hold of the argon fill gas test and Figure 17 shows the failure of the sensor during the temperature spike. Various locations along the fiber fail from temperatures of 720-730°C, there is a brief recovery when the temperature falls, but then the sensor fails and does not recover after the temperature increases again. The DTS fiber did not record any data after the failure in the argon fill, the vacuum and the nitrogen fill tests were conducted sequentially and as such did not result in meaningful data from the DTS fiber. The temperature profile over time until the sensor failure is show in Figure 18, the initial failure, recovery, then final failure can be seen through the temperature spike. The profile pf the hex block through transient heating is show in Figure 19, the red and green traces are both during the initial heat-up and the blue trace is during the steady state. The fiber at the time of the blue trace only reads leading up to the hex block and fails in the higher temperature regions.

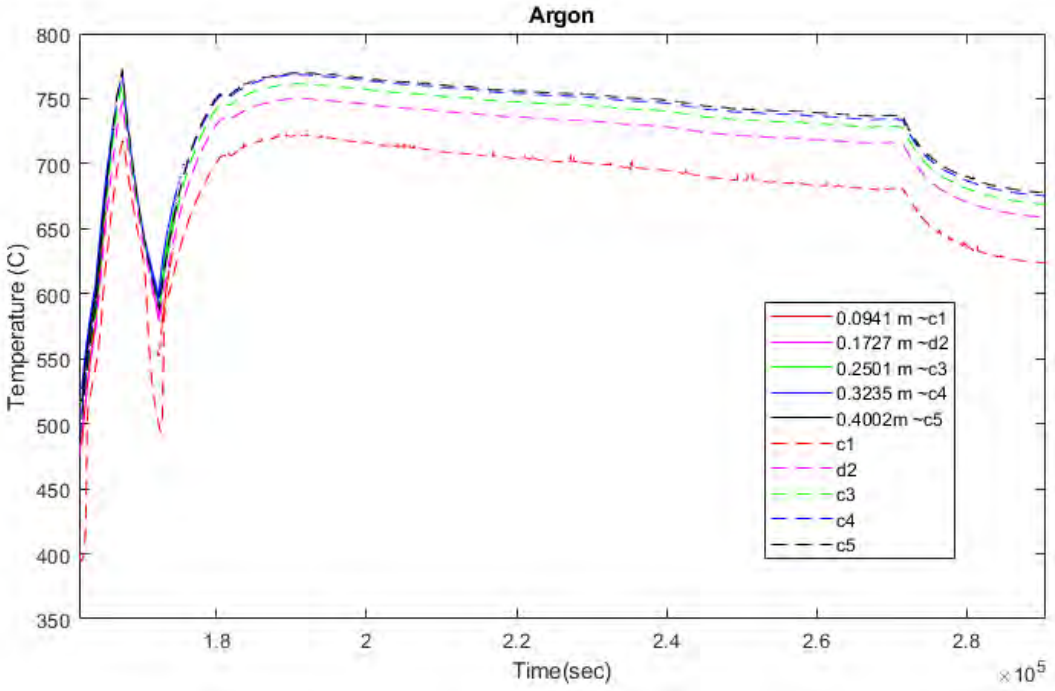

Figure 16: Initial steady state hold with argon fill gas.

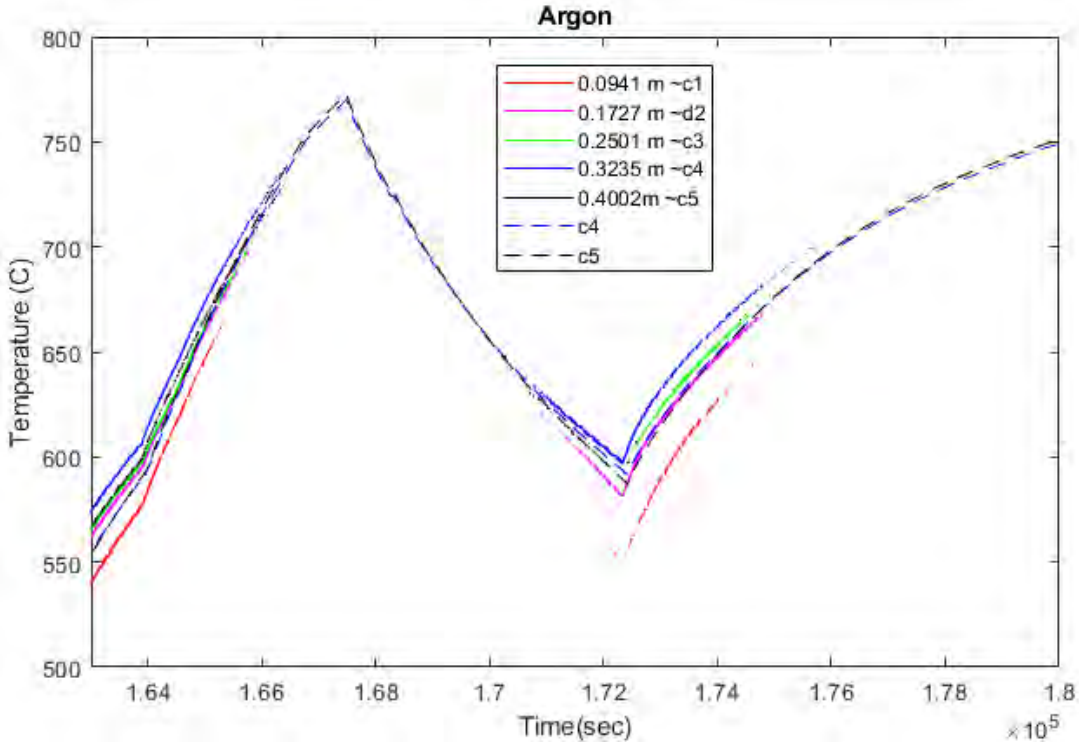

Figure 17: Temperature spike for argon fill gas heat-up.

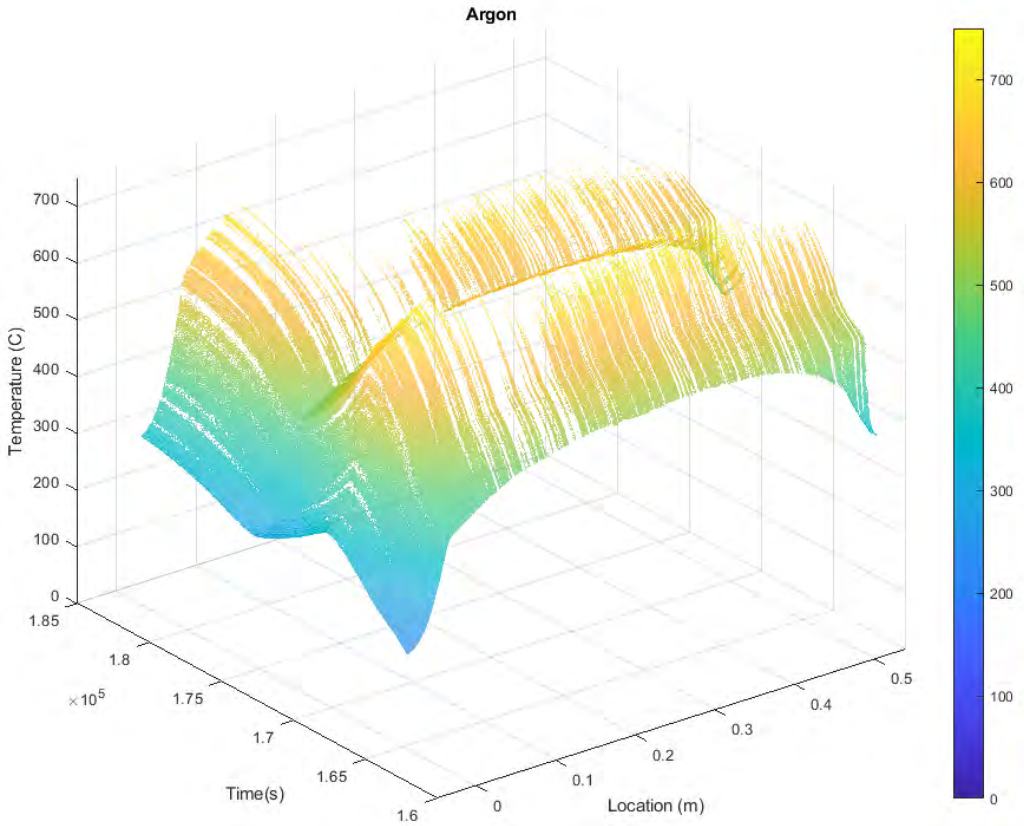

Figure 18: Full profile of the hex block until sensor failure of the argon fill test.

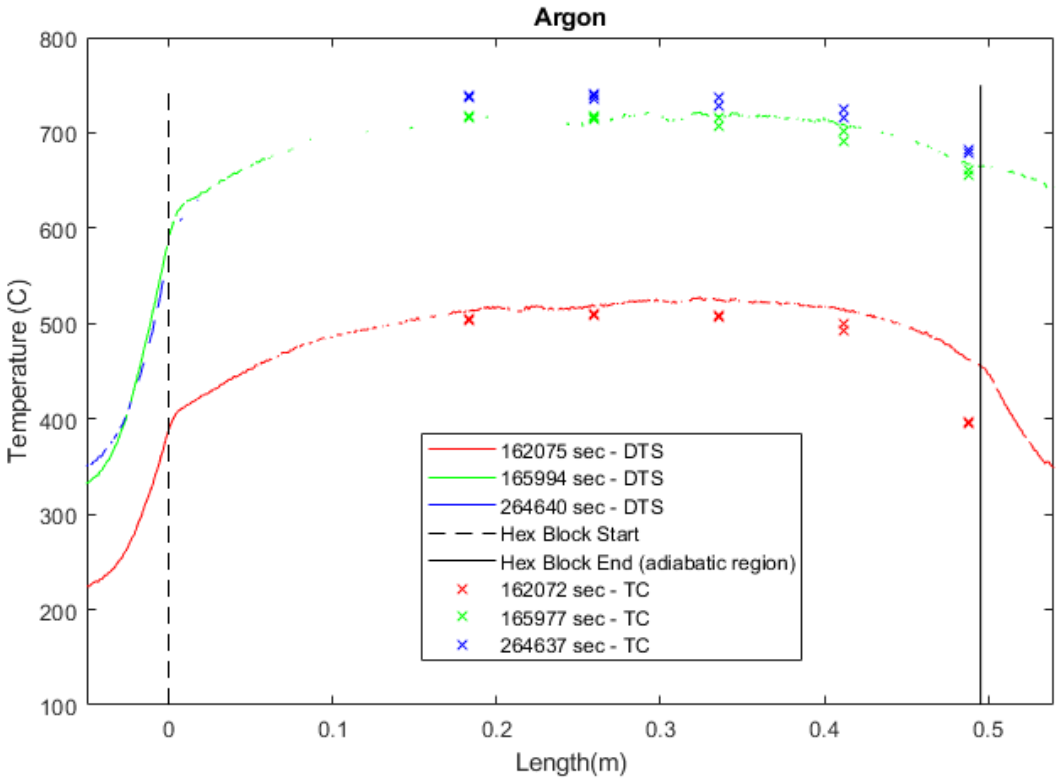

Figure 19: DTS fiber profile of the hex block at various times for the argon gas fill.

2.2 INL Sensor and Instrumentation for the Microreactor Agile Non-Nuclear Experimental Test Bed (MAGNET)

In addition to SPHERE, Idaho National Laboratory (INL) has established a 250 kW electrically heated, microreactor test bed to enable experimental evaluation of a variety of microreactor concepts. The Microreactor AGile Non-nuclear Experimental Test Bed (MAGNET) was constructed at INL to assist with the development, demonstration, and validation of microreactor components and systems. The purpose of this test bed is to support technology maturation that will reduce uncertainty and risk relative to the operation and deployment of this unique class of systems. The deployment of advanced sensor and instrumentation in MAGNET is scheduled for 2023 with the LANL fabricated eBlock37 heat pipe test article (Sweetland 2022).

2.2.1 Sensor and Instrumentation for eBlock37 Heat Pipe Test Article

This large-scale, multi-kW test article to be installed in MAGNET is an approximately 72-inch-long core block subassembly with 37 heat pipes and 54 cartridge heaters in the core, as shown in Figure 20. Total heater power for this assembly is 75 kW.

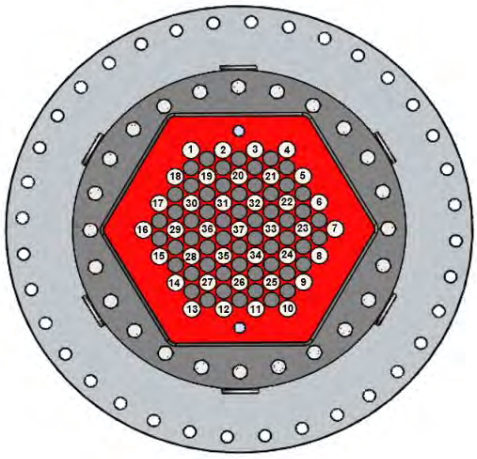

Figure 20 Cross section of the eBlock37 core37 block.

For the future testing of the eBlock37, the UT could be used to replace one or more thermocouples (single junction or multipoint). The areas of most interest would be measuring the evaporator exit temperature (Figure 21a), replacing core TCs (Figure 21 b), or measuring the wall temperature (Figure 21c). Fiber optic sensors would best be deployed in areas where there are many axial measurements being made in one location, Figure 22 shows examples of locations with multiple axial measurements, the outsides of the insulation and the heat exchanger walls. A single fiber could make many axial measurements, without increasing the space and mass of the sensor. This minimized the effect on the thermal properties of the measured system as well as fitting into small spaces if necessary. A fiber sensor would be particularly well-suited for them measurements of the outside of the insulation. Areas that maybe be insulated from the peak temperatures of the fuel but would benefit from high resolution or hot-spot detection would be good areas for the deployment of fiber optic temperature sensors.

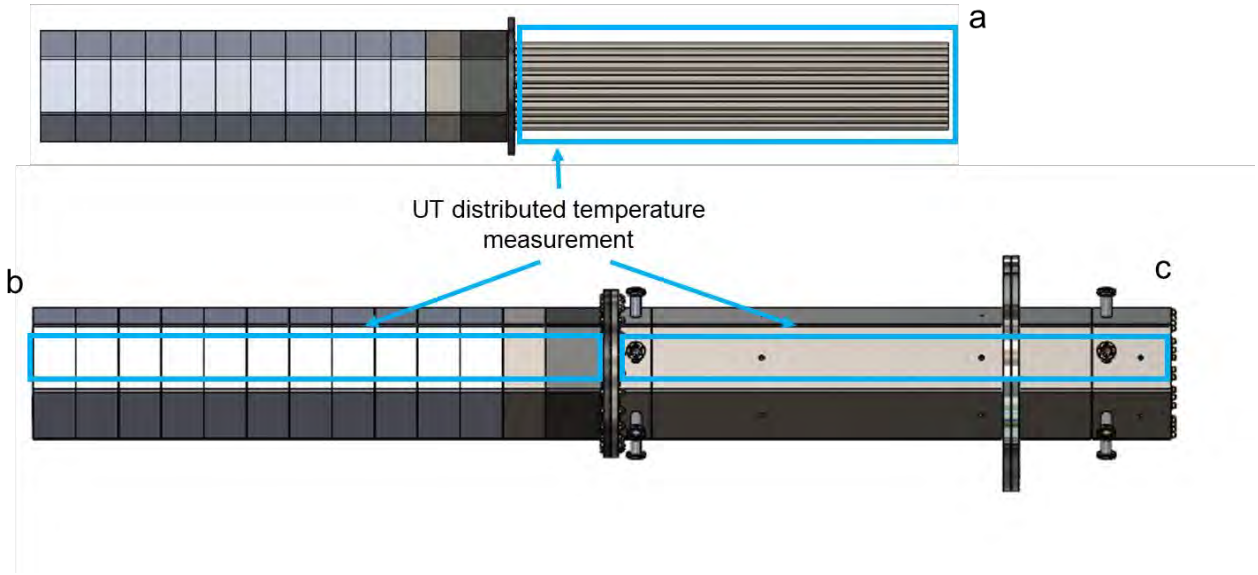

Figure 21. Possible locations for use of ultrasonic thermometer.

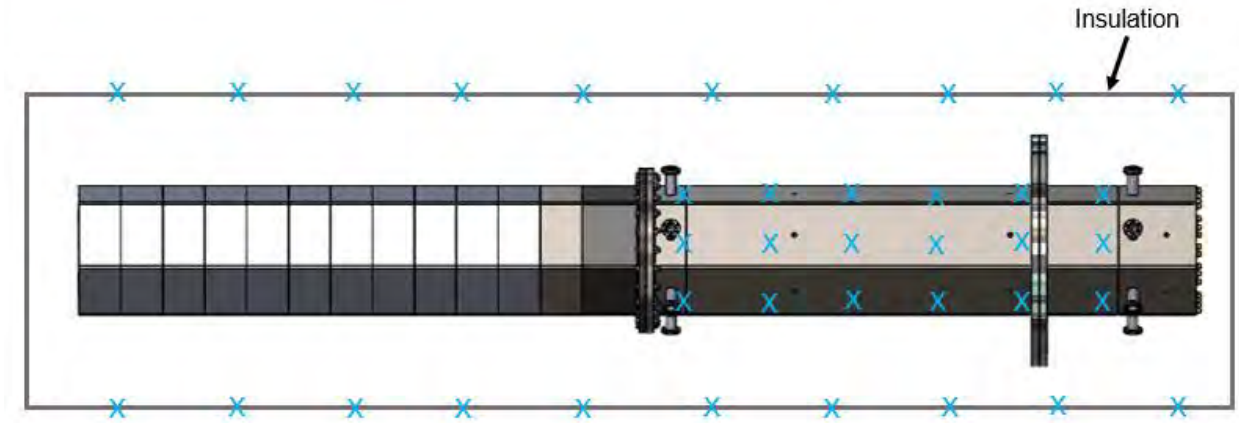

Figure 22: Possible locations for use of DTS or FBG fibers.

3. CONCLUSIONS

The INL sensor and instrumentation deployment activities have focused on testing the performance of a variety of distributed temperature sensors in representative microreactor reactor conditions. The data from advanced temperature sensors (fiber optics and ultrasonics) are in close alignment with traditional temperature sensors (thermocouples) and provide unique options for interested stakeholders that require temperature sensors beyond traditional single-point thermocouples. Future work will address identified issues noted for deployment in microreactor evaluations and will focus on deployment in larger tests including the eBlock37 test.

4. REFERENCES

1. Sabharwall, P., et. al, "DOE Microreactor Program: Summary of Experimental Capabilities Development and Activities," INL/EXT-20-60441, Idaho National Laboratory, June 2021.
2. Sabharwall, P., Hartvigsen, J., Morton, T., Sellers, Z., and Yoo, J.S., "SPHERE Assembly and Operation Demonstration," INL/EXT-20-60782, Idaho National Laboratory, December 2020.
3. Morton, T.J., "Microreactor Agile Non-Nuclear Experimental Test Bed (MAGNET) Startup," INL/EXT-20-61197, Idaho National Laboratory, December 2020.
4. McCary, K. M., "Evaluation of Fiber Bragg Grating and Distributed Optical Fiber Temperature Sensors," INL/EXT-17-41728, Idaho National Laboratory, April 2017.
5. Grobnic D., Smelser C.W., Mihailov S.J., Walker R.B., "Long-term thermal stability tests at 1000 °C of silica fibre Bragg gratings made with ultrafast laser radiation," Meas. Sci. Technol. 2006;17:1009–1013.
6. D. Sweeney, A. Schrell, and C. Petrie, "Compensation scheme for radiation-induced attenuation in optical fibers interrogated using low-coherence interferometry," Transactions of the American Nuclear Society 122, 291–294, 2020.
7. Daw, J., "Development of Ultrasonic Thermometer at INL," Nuclear Science User Facilities 2018 Annual Report: pp. 66-75, 2018.
8. Sweetland, K. and Reid B., "eBlock37 Instrumentation and Additional Controls," LANL presentation 12/15/2022.